Structure
Ways & Means

Observation of Decreased Radiation Damage at Higher Dose Rates in Room Temperature Protein Crystallography

Robert J. Southworth-Davies,[1] Melissa A. Medina,[1] Ian Carmichael,[2] and Elspeth F. Garman[1,*]
[1]Laboratory of Molecular Biophysics, Department of Biochemistry, Rex Richards Building, South Parks Road, Oxford, OX1 3QU, United Kingdom
[2]Notre Dame Radiation Laboratory, University of Notre Dame, Notre Dame, IN 46556, USA
*Correspondence: elspeth@biop.ox.ac.uk
DOI 10.1016/j.str.2007.10.013

SUMMARY

Radiation damage can be a problem when utilizing ionizing X-radiation in macromolecular crystallography. The dose dependence of radiation damage to eight lysozyme crystals at room temperature (292 K) was investigated in order to provide an accurate comparison with cryotemperature (100 K) results and to allow researchers to calculate expected maximum room-temperature-crystal lifetimes prior to data collection. Results of intensity-loss analysis unexpectedly showed that the dose tolerated by a crystal is dependent on the dose rate according to a positive linear relationship (99% correlation coefficient); a 60% increase in dose rate gave a 4-fold increase in crystal lifetime over the range studied. Alternative metrics of damage were also assessed from room temperature data. In the dose-rate range tested (6 Gy s^{-1} to 10 Gy s^{-1}), data collection at 100 K appears to offer a 26–113 times increase in the lifetime of the crystal.

INTRODUCTION

Prior to the use of cryocrystallographic techniques, X-ray diffraction experiments were historically carried out at room temperature (~292 K). At room temperature, it has long been observed that crystals are highly susceptible to the effects of radiation damage, often necessitating the use of many crystals to assemble a complete dataset. Attempts to mitigate these effects in macromolecular crystallography have been the driving force behind the development of cryocrystallography techniques. However, even at 100 K, radiation damage effects are observed in X-ray data collected at third generation synchrotron sources, which leads to a loss of the measured reflection intensities, ultimately resulting in lower resolution structures and sometimes to the inaccurate interpretation of biological results (Ravelli and Garman, 2006).

The first systematic study of radiation damage in protein crystals (carried out at room temperature) was performed on sperm-whale myoglobin by Blake and Phillips (1962). They found that the extent of radiation damage was proportional to the absorbed dose and deduced that a single 8 keV X-ray photon disrupts around 70 protein molecules and disorders a further 90 for doses up to about 20 Mrad (0.2 MGy, 1 Gy = 1 J kg^{-1} = 100 Rad). From their observations, they also suggested that specific structural damage was suffered by the protein molecule. All these conclusions were reached without knowledge of either the sequence or three dimensional structure of the protein.

Blake and Phillips investigated a particular class of reflections, those in the 010 zone, which corresponded to the centro-symmetric projection of the structure down the b axis of the unit cell. The reflections were measured row by row, starting with those at highest resolution (high θ), and the dose was about 5 Mrad (0.05 MGy) per set of reflections. X-rays were provided by filtered copper radiation from a sealed tube source. The same reflections were then measured repeatedly in the same order seven times, with a total dose of 50 Mrad (0.5 MGy) being absorbed by the sample. It was noted that the reflection intensities generally decreased as the dose increased, with the extent of the intensity loss being a function of $\sin^2\theta$ and being most marked for reflections at high angles. The expected intensity variation, corresponding to a random disordering of the structure (e.g., by increased thermal motion) was:

$$I = I_0 \exp\left(-\frac{B\sin^2\theta}{\lambda^2}\right) \quad (1)$$

where I corresponds to the measured intensity, I_0 is the initial intensity, B is a measure of disorder, θ is the angle of diffraction, and λ is the incident X-ray wavelength. However, upon plotting the relative intensity of each successive dataset versus resolution, it became obvious that this parameterization of intensity loss was inappropriate since it predicted that the intensity decrease should become more severe as $\sin\theta$ increased (if the structure was being disordered in an entirely random way), but in reality, it tended to level off as $\sin\theta$ increased. This led the authors to propose that following irradiation, the crystal consists of three components: (1) an undamaged fraction

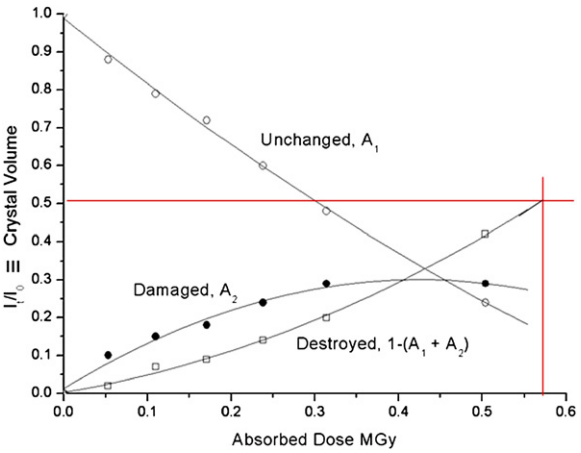

Figure 1. Results of Blake and Phillips' Measurements on Crystals of Myoglobin, See Introduction

The six points on each line correspond to the values of A_1, A_2, and $(1 - [A_1 + A_2])$ that were obtained from datasets 2–7 relative to dataset 1, showing the proportion of unchanged, damaged, and destroyed molecules, respectively, as a function of dose. The line in red indicates where half of the crystal has become amorphous. At this point, the summed diffraction intensity of the measured reflections was half of its initial value.

(A_1), which is entirely responsible for the remaining diffraction at high angles; (2) a highly disordered fraction (A_2), which contributes only to the diffraction at low angles; and (3) a thoroughly disorganized or amorphous part ($1 - [A_1 + A_2] = A_3$), which no longer contributes to the single crystal diffraction at all. They suggested that the resultant diffracted intensity at time t (I_t) is related to the initial intensity by the relationship:

$$\frac{I_t}{I_0} = A_1 + A_2 \exp\left(-\frac{B_2 \sin^2\theta}{\lambda^2}\right). \quad (2)$$

The values of A_1, A_2, and $(1 - [A_1 + A_2])$, which are time-dependent variables, were determined by fitting A_1 and A_2 in Equation 2 (with B_2 fixed at 40 Å^2) to the relative intensity versus resolution plot for each dataset. The values of A_1, A_2, and $(1 - [A_1 + A_2])$ were plotted as a function of dose (see Figure 1) and showed that after a dose of approximately 59 Mrad (0.59 MGy), 50% of the crystal had been rendered amorphous, 30% severely disordered, and 20% was unchanged. The undamaged fraction (A_1) shows an exponential decay for the first 20 Mrad (0.2 MGy: 100 hr of exposure) but for higher doses, this fraction of the crystal decreases more quickly than expected from a simple exponential decay, in accordance with a cumulative effect becoming dominant. The amorphous fraction ($1 - [A_1 + A_2]$) increases ever more quickly as the dose increases, while the partially disordered fraction (A_2) at first increases but then levels off. When the intensity measurements from the damaged crystal were corrected for radiation damage according to Equation 2, they agreed well with those from the relatively undamaged crystal. However, even after correction, it was noted that the relative intensities of different reflections at the same angle were not dependent on the angle of the reflection alone. The structure factors of some reflections increased slightly, whereas others decreased, leading to the deduction that specific structural damage to particular amino acid residues must be occurring within the crystal.

Following the work of Blake and Phillips, Hendrickson et al. (1973) investigated the decay of lamprey hemoglobin crystals and noted that over time (100 hr), the relative intensities of eight specific reflections showed a general decline, although individually they changed by different magnitudes and signs. To obtain a suitable correction for radiation damage based on more extensive information, the intensities of 150 reflections distributed evenly in resolution to 2 Å were then monitored as a function of dose. It was found that the average intensities declined approximately exponentially with time, showing greater decrease at higher values of sin θ/λ. These data conformed well to the relationship in Equation 2 deduced by Blake and Phillips.

Fletterick et al. (1976) made a radiation damage correction to diffraction data collected from glycogen phosphorylase *a* crystals, by making repeated measurements of ten strong reflections uniformly distributed at 2θ angles between 3° and 30°. An essentially monotonic decrease in diffracted intensity with time was observed for all the reflections, with a greater decrease exhibited for reflections at a higher scattering angle. This study led to the proposal of a modified model for radiation damage:

$$A_1 \overset{k1}{\rightarrow} A_2 \overset{k2}{\rightarrow} A_3 \quad (3)$$

where A_1 and A_2 are as in the Blake and Phillips nomenclature, A_3 is equivalent to $(1 - [A_1 + A_2])$, and k_1 and k_2 are the rate constants. The total time-dependent diffracted intensity, $I(t)$, was expressed as:

$$I(t) = \sum_{i=1}^{3} A_i(t) I_i \quad (4)$$

where i = 1, 2, or 3, A_i is as before, and the I_i values are related by the Fourier transform to the electron density for the ith state. This model was similar to the model of Blake and Phillips, except that direct transitions from A_1 to A_3 were not allowed ($k_3 = 0$). By interpreting these three states as being purely successive conformational transitions, the reaction kinetics become first order, with the variation of diffracted intensity as a function of time being described by:

$$I(t) = I_0 \left\{ \exp(-k_1 t) + \exp\left(-\frac{8\pi B \sin^2\theta}{\lambda^2}\right)\left(\frac{k_1}{k_1 - k_2}\right) \times (\exp(-k_2 t) - \exp(-k_1 t)) \right\}. \quad (5)$$

Hendrickson (1976) then derived an analytical expression for radiation damage in protein crystals based upon rate constants for all possible paths in the Blake and Phillips model of Equation 6. He tested this general model, together with the $k_2 = k_3$ model (Hendrickson et al.,

1973), the $k_1 = k_2$ and $k_3 = 0$ model, the $k_3 = 0$ model (Fletterick et al., 1976), the $k_1 + k_3 = k_2$ model (Hendrickson, 1976), and the arbitrary time-dependence model (Blake and Phillips, 1962) against the Blake and Phillips experimental data from myoglobin. The possible transition paths between components in the Blake and Phillips model are:

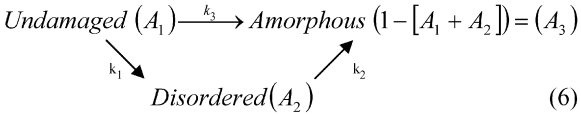

(6)

and Hendrickson concluded that all models explained the data well at moderate damage/dose (90 hr and 26% I/I_0 decrease). Although none of the models explains the data at very high dose (266 hr exposure and 72% I/I_0 decrease), at high levels of damage (up to 47% I/I_0 decrease after 164 hr exposure), the damage is still very well described by the $k_3 = 0$ Fletterick et al. (1976) model, thus apparently showing that damage is a sequential process as described by Equation 3 whereby the molecular structure is first disordered by one event and then effectively denatured by a second event.

This $k_3 = 0$ radiation damage model was later extended (Sygusch and Allaire, 1988) by adding a dose-dependent stage A'_1, between the undamaged and the damaged stages that conformationally resembles the undamaged state, thus still contributing to diffraction at all angles.

$$A_1 \xrightarrow{k_0} A'_1 \xrightarrow{k_1} A_2 \xrightarrow{k_2} A_3. \quad (7)$$

It characterizes radiation damage in terms of successive conformational transitions of the protein from an undamaged to a spatially disordered and then finally to an amorphous state. Unlike the $k_3 = 0$ model, this description provided a good fit for the intensity decay of reflections even up to high levels of radiation damage.

The models described above were thought to provide the most appropriate corrections for radiation damage occurring in protein crystals irradiated at room temperature. The radiation damage consists of two distinct components; primary and secondary. Primary damage (which cannot be avoided) is the direct ionization of an atom by an X-ray photon (photoelectric absorption) and Compton (inelastic) scattering. The absorbed energy is not uniformly distributed within the sample but is deposited inhomogeneously as scattered spurs in amounts of 20–100 eV (Singh and Singh, 1982). Secondary radiation damage derives from the formation of up to 500 secondary electrons, with mean track lengths of a few micrometers (if using 12 keV [1.03 Å] photons), that will induce further excitation and ionization events within the atoms of the crystal (O'Neill et al., 2002).

Various techniques have been developed to try to mitigate radiation damage occurring in X-ray diffraction experiments. It was noted in 1958 that the resolution of diffraction was limited by temperature-dependent dynamic disorder in the protein (King, 1958). In 1970, two particular reflections in X-ray diffraction experiments on lactate dehydrogenase were monitored at 298 K and 198 K, and it was observed that the intensity decay of the reflections with accumulated dose was much less at the lower temperature (Haas and Rossmann, 1970). This led to the development of the radiation damage mitigating technique of cryocooling (Hope, 1988; Garman and Schneider, 1997; Rodgers, 1997; Garman, 1999). Protein crystals are now routinely flash cooled to 77 K or 100 K and held at 100 K during most X-ray diffraction experiments. From analogy with observations in electron microscopy (for 100 keV electrons), a dose limit of 2×10^7 Gy for a cryocooled protein crystal was calculated by Henderson (1990) being the dose sufficient to cause the summed X-ray diffraction pattern to fall to half of its original intensity ($D_{1/2}$). Henderson used the fading of the diffraction pattern during electron irradiation of 2D protein crystals to measure destruction of the crystalline atomic arrangement by ionizing radiation. Radiation chemical studies with electrons and hard X-rays of energy above 100 keV show reasonably close agreement of the amount of energy deposited per unit mass by these two types of ionizing radiation. Electron diffraction patterns of protein crystals typically fade to half of their original intensity after about one electron $Å^{-2}$ irradiation at room temperature or five to ten electrons $Å^{-2}$ at 77 K. This electron dose is roughly the same for a wide variety of organic and biological specimens. The value of five electrons $Å^{-2}$ is equivalent to a dose of 5×10^7 Gy. Henderson suggested that in the first part of the depth-dose curve, this might be two to three times less, resulting in the so-called "Henderson limit" of 2×10^7 Gy for the $D_{1/2}$ of protein crystals (Henderson, 1990). More recently Owen et al. (2006) have published an experimental study of the X-ray radiation damage dose limit for cryocooled (100 K) protein crystals in which it was found that the total intensity of diffraction had a linear dependence on absorbed dose. The dose required to halve the intensity of the diffraction pattern was 4.3×10^7 Gy but an upper limit of 3×10^7 Gy was suggested ($I = 0.7\ I_0$), beyond which point the biological information obtained from the experiment might be compromised. The experiments were performed on several crystals of the iron storage protein holo- and apoferritin (the iron loaded and empty forms, respectively) and produced highly reproducible results.

However, even though the dose limit has now been measured at cryotemperatures, the same is not true at room temperature. The advantage that cryotemperature experiments provide in terms of expected lifetimes of the crystal in the X-ray beam is also currently unknown except for an ad hoc estimation that compares the experimental limit of 4.3×10^7 Gy at cryo temperatures with that of the Blake and Phillips room temperature data (0.059×10^7 Gy, when the destroyed part of the crystal reaches 50%). This provides an estimate of increased lifetime at 100 K relative to room temperature of around a factor of 70 (Nave and Garman, 2005). The investigation reported here was undertaken to establish a radiation damage dose limit for room temperature X-ray crystallography both to provide a quantitative comparison with

cryotemperature results and to allow planning of room temperature experiments.

The loss of the total diffraction intensity provides a means of monitoring radiation damage in a crystal. Another promising radiation damage metric at cryotemperatures has recently been suggested. Experiments carried out on cryocooled lysozyme crystals were analyzed in terms of the isotropic B factor (B_{rel}), and a coefficient of sensitivity, S_{AD}, ($S_{AD} = \Delta B_{rel}/\Delta D 8\pi^2$, where $\Delta B_{rel}/8\pi^2$ is the change in relative isotropic B factor, and ΔD is the change in dose) was defined and found to be a robust measure for radiation damage and linearly dependent on it. This coefficient relates the increase in mean-squared atomic displacements to the dose (Kmetko et al., 2006).

In the present study, the metric I/I_0 was used to parameterize the level radiation damage observed at room temperature (292 K) for between five and eight successive datasets collected from each of eight crystals of chicken egg white lysozyme (HEWL). The B_{rel} of all the datasets from each crystal were also calculated to investigate if B_{rel} or S_{AD} would display a similar behavior (linear increase of B_{rel} with dose; a constant S_{AD}) at room temperature to that observed at cryotemperature (Kmetko et al., 2006) and thus be a suitable metric for radiation damage studies at room temperature. The unit cell volume and specific structural damage were also examined as a function of dose.

RESULTS

Radiation Damage to Each Crystal

Figure 2A shows the changes in the relative intensities between 40 Å and 2 Å of all reflections from the eight separate lysozyme crystals as a function of absorbed dose. The values of I/I_o were calculated from the *Mn(Imean)* values obtained from SCALA of each dataset relative to the first dataset for that crystal. *Mn(Imean)* includes intensity data from both fully recorded and summed reflections. Each of the crystals 1 to 7 was subjected to a different dose rate. The dose rate for crystal 8 was as closely matched as possible to the dose rate for crystal 2 but datasets were collected discontinuously rather than continuously (see Experimental Procedures section). The rates of summed intensity decay show a first order dependence, as was previously observed in the room temperature radiation damage study of Blake and Phillips (see Figure 1). To check for any resolution dependence of the decay observed in our study, the intensity data for crystals 2 and 3 were divided into three different resolution shells (10–6 Å, 6–4 Å, and 4–2 Å) and replotted as a function of dose (data not shown). There was no observed resolution dependence: the different bins very closely bracketed the total intensity decay.

To confirm the first order nature of the rate of intensity decay (Figure 2A), the negative natural logarithms of the relative intensities for each crystal were plotted against the dose, resulting in linear increases, all with correlation coefficients of above 97.7% (Figure 2B). The most striking feature of this plot is that the rate of the intensity loss varies

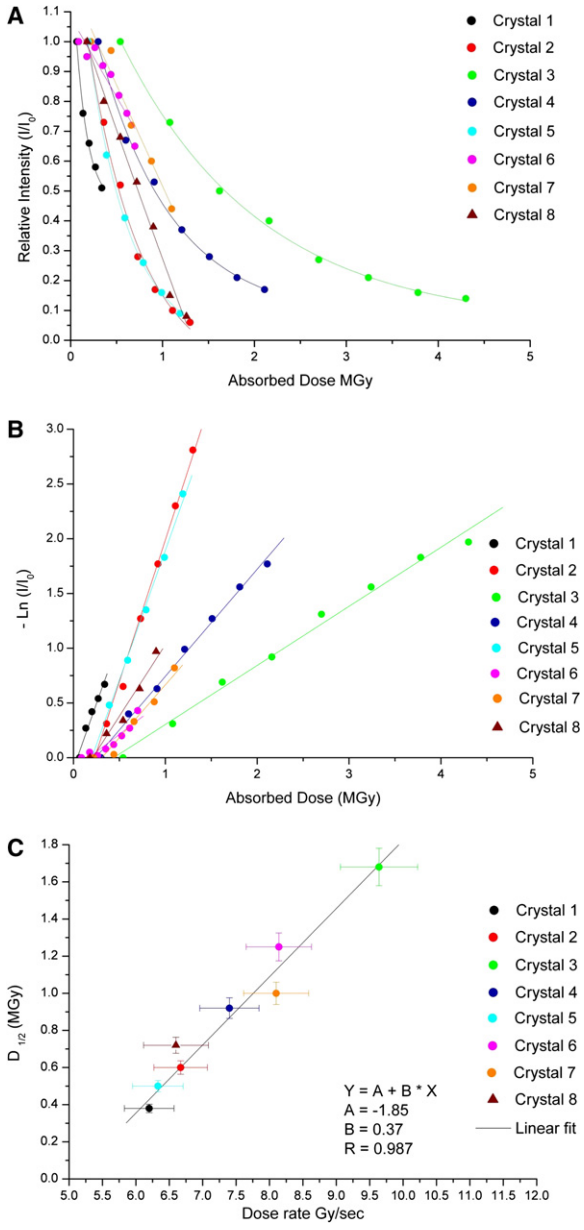

Figure 2. Observation of Reduced Radiation Damage at Higher Dose Rates in RT Protein Crystallography

(A) Relative summed intensity plot for all eight HEWL crystals against absorbed dose.

(B) The negative natural logarithm of the relative intensity decay against absorbed dose. The linear functions reveal that the process is first order.

(C) Dose-rate dependence of $D_{1/2}$ of the eight crystals tested. The correlation coefficient of 0.99 shows that there is a positive linear dependence of $D_{1/2}$ on the dose rate, a so called "inverse dose-rate effect." The errors shown represent the error on the dose calculations due to the estimated uncertainties in measured crystal sizes, the beam profile, and the beam size (total of ±6% in x and y). They do not include the possible systematic error on the diode calibration (estimated at 5% from cross calibration against two other calibrated diodes) since this error will affect all doses and dose rates by the same proportion.

significantly between the eight different crystals, with up to a factor of five difference between the $D_{1/2}$ of crystal 1 and 3.

Dose-Rate Dependence of Radiation Damage

Due to the observed variation in $D_{1/2}$ for the eight crystals, an investigation was carried out to establish if a dose-rate dependence existed. A possible dose-rate dependence had been noted in previous studies at room temperature when moving from a rotating anode to a synchrotron source (Wilson et al., 1983).

When the rate at which the X-radiation was absorbed by the crystal in Gy s^{-1} was plotted (calculated from the total X-ray exposure time, not from the total time involved) against the $D_{1/2}$ for the eight crystals, a linear dependence (Figure 2C) is very clear. There is a strong, positive correlation coefficient (R = 98.7%) between $D_{1/2}$ and dose rate, so that a higher dose rate leads to the crystal being able to withstand a higher absorbed X-ray dose. Quantitatively, for this case, a 60% increase in the dose rate leads to a 4-fold increase in the resultant $D_{1/2}$.

Unit-Cell-Volume Dependence with Radiation Damage

The unit-cell volume was plotted against the absorbed dose (data not shown). Comparisons between the crystals show no systematic changes in the unit-cell volumes, and the changes recorded were, at the most, only 1.6%. The unit-cell volume is therefore not a suitable metric for radiation damage at room temperature, in agreement with the investigations of this parameter as a radiation damage metric at 100 K (Murray and Garman, 2002; Ravelli et al., 2002). Previous work at room temperature on holoferritin microcrystals of around 3 μm showed a collapse of unit-cell volume of up to 55% when exposed to very high X-ray flux (Boutet and Robinson, 2006), but both the doses and flux used in these experiments are far higher than those used in our work.

Relative B Factors

The relative isotropic B factors (B_{rel}) for all the datasets from each crystal were obtained with SCALEIT. The B_{rel} were extracted from the log file as the RMS differences between the native (first) dataset and the derivative (subsequent) datasets calculated before Wilson scaling. A plot of B_{rel} for each crystal against dose showed an increase with radiation damage, but that the rates of increase vary from crystal to crystal and the increase with dose was not consistently linear (data not shown). At cryotemperatures, the B_{rel} has been observed to increase linearly with dose (Kmetko et al., 2006).

In order to see if, as with the intensities, this variation is dose-rate dependent, the coefficient of sensitivity, S_{AD}, was calculated and also plotted against the dose rate. If this was a valid metric, we would have expected S_{AD} to show a negative sloped correlation to the dose rate, as a higher dose rate leads to a lower rate of damage. The resultant scatter plot (data not shown) showed no correlation, leading us to the conclusion that the coefficient of sensitivity is not a useful indicator for radiation damage at room temperature.

DISCUSSION

Within the range of dose rates tested (6–10 Gy s^{-1}), the HEWL crystals required 0.38–1.63 MGy for the summed intensity to decay to half of the initial diffraction intensity. Compared to the $D_{1/2}$ limit of 43 MGy measured at cryotemperature (100 K) by Owen et al. (2006), our results suggest that cryocooling to 100 K provides a lifetime increase of between 26–113 times. This range encompasses the previous estimate of 70 (Nave and Garman, 2005) for the improvement in crystal lifetime upon cryocooling.

It is thus not possible to provide a single $D_{1/2}$ dose limit for room temperature experiments, in contrast to cryotemperature crystallography. Our results show that radiation damage at room temperature depends on the dose rate and not just on the absorbed dose. This finding helps rationalize previous room temperature observations at synchrotrons, where longer protein crystal lifetimes were obtained than on sealed tube and rotating anode sources (Phillips et al., 1976; Wilson et al., 1983). Wilson et al. (1983), in a study involving three different protein crystals (glycogen phosphorylase *b*, β-lactamase I, and troponin C to 2 Å, 2.5 Å, and 6 Å resolution, respectively) at an incident wavelength of 1.54 Å, noted that there was a 5-fold increase in crystal lifetime when data were recorded at the 1.85 GeV DCI storage ring at LURE compared to data recorded with a conventional rotating-anode source.

Previous work on dose/dose-rate effects at cryotemperatures have indicated that only a small dose rate effect is evident at the flux densities currently being utilized for macromolecular crystallography at synchrotrons (Leiros et al., 2001, 2006; Ravelli et al., 2002; Owen et al., 2006; Sliz et al., 2003). Owen et al. (2006) found that at cryotemperature, the relative decrease in summed intensity of the diffraction pattern showed a linear response to the dose absorbed by the crystal. However, the size of any dose-rate effect was small, with a higher dose rate lowering $D_{1/2}$, in direct contrast with the response observed in our room temperature study where the opposite is true. In the Owen et al. (2006) study, a 10-fold increase in the dose rate (0.4×10^4 Gy s^{-1} to 4.0×10^4 Gy s^{-1}) only resulted in a 10% reduction in $D_{1/2}$ for apoferritin, which is a typical protein in terms of its atomic composition. In the extreme case of the iron loaded holoferritin, which has the highest known ratio of metal atoms to amino acid content of any protein (1 to 2), a 10% reduction in $D_{1/2}$ was seen with a 3-fold increase in dose rate. Leiros et al. (2006) found that there was no clear dose-rate effect on the global indicators of radiation damage but that there was a small measurable dose rate effect observed (a higher dose rate resulting in greater damage) when monitoring specific structural radiation damage. They noted that at cryotemperature, the dose rate affects specific radiation damage far less than does the total absorbed dose. Sliz et al. (2003) studied the overall effect of dose rate on X-ray diffraction intensities by monitoring changes in R_{merge} and

I(t)/I(0) for crystals of three different proteins. They concluded that for flux densities up to 10^{15} ph s^{-1} mm^{-2}, radiation damage at the macroscopic level is proportional to the total dose and is not dependent on the dose rate. In contrast, Ravelli et al. (2002) found a dose-rate-dependent increase in unit-cell parameters for holoferritin but explained this as possibly due to sample heating because of the especially high content of iron in the core.

These small dose-rate effects observed at cryotemperatures are classified in radiation biology as "normal," i.e., an increase in dose rate induces a higher rate of damage per unit dose. On the other hand, if increasing the dose rate causes the sample to suffer lower damage per unit dose, then this is known as an "inverse dose-rate effect."

The only room temperature study comparable with the work presented here is that of Cherezov et al. (2002), who noted both inverse dose-rate and normal dose-rate effects in the study of lipidic mesophases (liquid-crystalline phases). They attributed the different responses to absorbed dose to two types of damage (type 1 and type 2). Type 1 damage (disordering of lamellar stacking) was observed when the loss of diffraction at low angles was monitored as a function of accumulated dose over the dose rate range 2–640 krad s^{-1} (20–6,400 Gy s^{-1}) for fully hydrated (minimum 50% w/w water) dipalmitoylphosphatidylcholine (DPPC) in the $L_{\beta'}$ phase on ID2 (ESRF) at 298 K, resulting in an inverse dose-rate effect. Type 2 damage (a dramatic-phase transformation) was observed when water stressed (i.e., lower than 50% w/w water) dipalmitoleoylphosphatidylethanolamine (DiPOPE) in the L_{α} phase was examined. They postulated that the two distinct behaviors could arise from the differences in the chemistry and mobility of free radicals in the two types of lipidic systems under investigation.

The relative summed intensity changes of their type 1 samples measured at different dose rates that were reported in their paper have been replotted in Figure 3A. Using their data, we have also plotted a new figure, $D_{1/2}$ versus dose rate (Figure 3B). It can be seen that the relative intensity loss shows the same trend as our data, with the highest dose rate resulting in the largest $D_{1/2}$. Furthermore, the data show a linear dependence of $D_{1/2}$ on dose rate (correlation coefficient 99%) in agreement with our results for crystalline samples. Cherezov et al. (2002) suggested that the lipids were undergoing peroxidation reactions whose free radical chemistry contributed to the unusual inverse dose-rate effect. Other studies observing inverse dose-rate effects in biological samples include those on lipids (Stark, 1991), proteins in the presence of lipids (Koufen et al., 2000), human erythrocytes (Krokosz et al., 2006), and radiobiological studies involving neutrons (Hill et al., 1982, 1984; Sykes and Watt, 1989).

It is necessary to attempt to deconvolute the inverse dose-rate effect observed in our experiments from a possible time dependence of the damage progression, as the crystals measured at higher dose rates will have been exposed for a shorter total time per absorbed dose. To deconvolute the two effects, crystal 8 was tested at the same dose rate as crystal 2, but instead of recording the data-

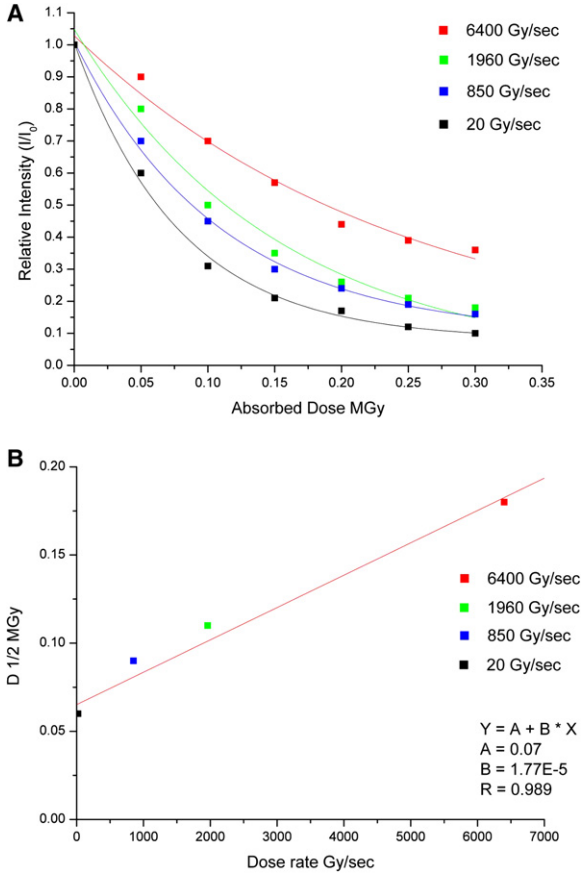

Figure 3. Observation of Reduced Radiation Damage at Higher Dose Rates Observed for Lipidic Mesophases

(A) The damage to hydrated dipalmitoylphosphatidylcholine at 50% w/w water at 298 K as a function of accumulated dose shown at four different dose rates; data reproduced with permission from Figure 14 of Cherezov et al. (2002) (http://journals.iucr.org/).

(B) Dependence of damage ($D_{1/2}$) on dose rate of hydrated dipalmitoylphosphatidylcholine at 50% w/w water at 298 K extracted from the data shown in Figure 3A.

sets continuously, a pause of 10 hr 50 min (the time for collection of one dataset for crystal 2) was allowed between each dataset. The average dose per total time was thus reduced, but the dose per unit irradiation time was the same. $D_{1/2}$ for crystals 2 and 8 was found to be the same within the stated error limits (see Figure 2C), thus ruling out elapsed time as a significant contributor to the dose-rate dependence of $D_{1/2}$. A continuous versus discontinuous exposure experiment has in fact already been carried out on lipidic mesophases (see above) (Cherezov et al., 2002). They observed an inverse dose-rate effect under both continuous and discontinuous irradiation; thus their results also indicate that elapsed time is not a significant factor in the $D_{1/2}$ dependence on dose rate.

In cryotemperature crystallography, it is known that secondary damage is not eliminated completely at 100 K as the order of specific structural damage in the absence of heavy atoms does not depend on the absorption coefficient of the atoms. If it did, the order of damage to

particular amino acid residues would be the disulphides followed by the methionine residues. Instead, the observed order of damage is to disulphide bonds followed by glutamates and aspartates and the loss of OH moieties from tyrosine residues (Burmeister, 2000; Ravelli and McSweeney, 2000; Weik et al., 2000).

The proportion of secondary damage in a protein crystal will increase as the temperature is raised from cryotemperatures toward room temperature since the radicals will gain mobility. The overall radiation chemistry may thus be very different at room and cryotemperatures, with the room temperature chemistry being significantly affected by those species that would have been immobile at 100 K. The effect of crystal heating at room temperature by the X-ray beam is not thought to be a significant factor when considering the possible mechanisms of damage. Measurements using an infrared camera of the rise in temperature of a 1 mm diameter glass bead at 300 K with no nitrogen cooling when irradiated with a 6.5 keV X-ray beam of 3.24×10^{12} ph s^{-1}, and size 0.103 mm (FWHM horizontal) by 0.084 mm (FWHM vertical), showed a rise of only 22 K before reaching a steady state (Snell et al., 2007). The flux and flux density for these measurements were respectively a factor of 10^4 and 1.7×10^4 larger than those used in our study.

In fact, from an analysis of the specific structural features seen in the F_{o1}-F_{ox} electron density maps obtained in our study, it is clear that disulphide bonds are the first to be damaged at room temperature, as reported previously (Helliwell, 1988). Unlike the changes seen at 100 K, there is no clear evidence in our maps for damage to residues other than disulphides (Figure S1, see the Supplemental Data available with this article online). Due to high levels of noise, the interpretation of the room temperature electron density maps from sequential datasets was in general much more difficult than for the equivalent maps generated by experiments at cryotemperatures. Sources of this noise may be the overall degradation of the crystal and/or by the change in the structure in the course of a single dataset.

Typically, the energy imparted by X-irradiation is deposited in isolated (separation ~500 nm) spurs (diameter ~5 nm) along the radiation track (Mozumder and Magee, 1966). Due to the high solvent content of macromolecular crystals (39% by volume for lysozyme), many of the initial radicals produced as a result of this energy deposition will come from the radiolysis of the solvent—in our case water. The resulting excitation and ionization of the water molecules leads to the formation of electrons, hydronium ions, hydroxyl radicals, and hydrogen atoms on the picosecond time scale. At room temperature and neutral pH, the yields of hydrated electrons and hydroxyl radicals are approximately equal, while the yield of hydrogen atoms is much smaller. However, at acidic pH, hydrated electrons are rapidly converted to hydrogen atoms. After intraspur recombination (i.e., at times on the order of several tens of nanoseconds), G values (number of species per 100 eV of energy deposited) of 2.7 have been estimated for both the reducing and oxidizing species (LaVerne, 2000; Pimblott et al., 1996). These reactive radicals are then available for homogeneous diffusive interactions, and small yields of the eventual molecular products, H_2 and H_2O_2, are already present.

The primary oxidizing radical, $HO^{\cdot}$, is highly reactive, abstracting hydrogen atoms from C-H and N-H bonds, to form carbon- and/or nitrogen-centered radicals, which in turn will scavenge any nearby molecular oxygen. Other reactive channels involving $HO^{\cdot}$ include addition to unsaturated linkages such as those present in aromatic amino acids and electron capture from suitable donors to form the relatively stable hydroxide ion. Even for simple amino acids, the detailed course and outcome of $HO^{\cdot}$-induced oxidation is rather complex (Bonifacic et al., 2000; Hug et al., 2000; Wisniowski et al., 2002).

Both reducing radicals, the hydrated electron and the hydrogen atom, react rapidly in the presence of oxygen yielding $O_2^{-\cdot}$ or $HO_2^{\cdot}$ depending on the pH (the radical pK_a is 4.6). These oxygen-centered radicals (in addition to hydrogen peroxide formed for example by radical intercombination) can also then go on to attack the components of the protein.

One suggested explanation of the observed inverse dose-rate effect is that at low dose rates, the radicals produced react preferentially with neighboring molecules resulting in the initiation of a cascade of reactions causing damage within the protein crystal. At high dose rate, radical recombination becomes increasingly important in our room temperature experiments, thus reducing the extent of the observed damage. This mechanism also provides a plausible explanation for the results of Cherezov et al. (2002).

Conclusions

The decay of the total diffraction intensity with dose of eight lysozyme crystals at room temperature was found to be first order in nature, in concordance with the results of Blake and Phillips (1962) obtained from myoglobin crystals. However, our study surprisingly showed that for data collection at room temperature, a strong positive linear (correlation coefficient 99%) dose rate pertains: a longer crystal lifetime is obtained by using a higher dose rate, with a 60% increase in the dose rate leading to a 4-fold increase in the dose required for the summed diffraction intensity to fall to half of its original value. Our results provide rationalization for previous observations (Phillips et al., 1976; Wilson et al., 1983) and also for anecdotal evidence in the crystallography community that at room temperature, protein crystals appeared to have longer lifetimes at synchrotrons as compared to typical rotating anode home sources.

Over the dose-rate range tested (6–10 Gy s^{-1}), our results suggest that cryocooling to 100 K provides a lifetime increase of approximately 25–110 times, bracketing the previous estimate of 70 (Nave and Garman, 2005). These findings have direct relevance to room temperature data-collection protocols. For example, the crystallographic study of viruses is often hampered at cryotemperatures because of an unacceptable increase in the mosaicity

suffered by some crystals on cryocooling; consequently the crystals are irradiated at room temperature. There are also some laboratories around the world that currently do not have access to cryogenic facilities and thus routinely collect room temperature data. Work is currently in progress to determine if these results can be extrapolated over a wider range of dose rates, encompassing values obtained with highly attenuated synchrotron beams.

EXPERIMENTAL PROCEDURES

Crystal Preparation

HEWL was obtained from Sigma (L6876) and was crystallized by hanging drop vapor diffusion. The well solution (400 μl) was composed of 10% w/v NaCl in 200 mM sodium acetate at pH 4.7. The required pH was obtained with 1 M HCl by using a calibrated Schott CG840 pH meter. The protein solution (4 μl) contained 50 mg/ml^{-1} HEWL in 200 mM sodium acetate, and the suspended drop contained 4 μl of well solution and 4 μl of protein solution. The crystals, of space group $P4_32_12$, ranged in size between 0.001 mm^3 and 0.53 mm^3 and took between 1 and 3 days to grow.

Crystal Mounting

Crystals for room temperature data collection were mounted in three slightly different ways. The first method used a cryo-loop (Teng, 1990) on an Oxford Cryosystems nickel top hat, and a 2 cm long thin quartz capillary (2 mm diameter) was lowered over the crystal and pin. This was pushed into plasticine (modeling clay) that was placed around the base of the top hat (Skrzypczak-Jankun et al., 1996). Mother liquor was injected into the capillary above the loop-mounted crystal, to prevent the crystal drying out in the loop. The top of the capillary was then sealed with a small amount of dental wax. The top hat with capillary was then mounted as usual on the in-house X-ray source, and datasets were recorded.

In the second method, litholoops (etched mylar supplied by Molecular Dimensions) were employed. They were mounted in the same way as the cryoloop but had the added advantage of being stiffer and unlike the cryoloop, could not unravel.

For the third mounting method, the MiTeGen mounting system (Kalinin et al., 2005) was used, in which a plastic rather than a quartz capillary is placed over the crystal. The plastic tube was more easily cut to the required length, and instead of cryoloop mounting, the crystal was picked up with a premounted plastic scoop. Both ends of the plastic tube were sealed with vacuum grease. Occasionally, some of the loop-mounted experiments suffered from crystal dehydration, so a single crystal was wall mounted on the side of a thin quartz capillary in a small drop of the mother liquor (Basavappa et al., 2003), to act as a reference crystal that definitely remained hydrated throughout the experiment.

The method of mounting and orientations of the crystals produced no detectable difference in the results obtained. The dose absorbed by a crystal is almost independent of the crystal depth, z, through which the beam passes. This is because the absorption path length of the crystal for 8–14 keV X-rays is large compared to typical crystal sizes (Murray et al., 2005).

Data Collection

Data were collected (Table 1) with a Rigaku RU200H rotating copper anode generator producing 1.54 Å (8.05 keV) X-rays and with a 345 mm diameter Mar imaging plate detector. The generator is equipped with converging blue Osmic multilayer optics. In addition to the benefit of high X-ray flux, these also provide a reasonably convergent beam with a small size and good spectral purity.

The slits closest to the crystal position were set to 1.0 mm × 1.0 mm resulting in a beam size at the crystal position of 0.5 mm (0.24 mm full width half maximum [FWHM]) horizontally and 0.3 mm (0.1 mm FWHM) vertically. The crystal-to-detector distance ranged from 160 mm to 180 mm. Each crystal of HEWL was subjected to repeated sweeps of between 45° and 90° in ϕ, each sweep consisting of 50–225 images of 120–800 s exposure and $\Delta\phi$ of 0.4°–1.0° per image. Crystals 1 to 7 were exposed to X-rays under a "continuous" collection regime whereby sequential datasets were recorded in immediate succession. Note that the irradiation of the crystal under these conditions is not continuous since the Mar345 imaging plate detector takes 90 s to read out after each image, during which time the crystal is not irradiated. Crystal 8 was subject to a "discontinuous" dataset collection regime; the collection of each dataset was separated by a time equal to that required for a single dataset (10 hr 50 min). For each new crystal, two test images of the crystal were taken 90° apart in phi and then analyzed with the STRATEGY option of MOSFLM (Leslie, 2006) in order to determine the optimum rotation angle and maximum data completeness.

Dose Calculations

The program RADDOSE (Murray et al., 2004) was used to calculate the total absorbed dose (Table 1) in Gray (J kg^{-1}). It uses the measured crystal size, beam size and profile, photon flux, total exposure time, and atomic contents of the crystal to calculate the absorption coefficient of the sample and thus the number of photons absorbed by the crystal. This is then converted into the energy deposited, which is then divided by the mass of the exposed part to give the absorbed dose in Gray. Both the amino acids of the protein molecules and any heavy atoms present in the crystal will contribute to the absorption of X-ray photons. An average amino acid is defined by RADDOSE to contain: 5 carbon, 1.3 nitrogen, 1.5 oxygen, and 8 hydrogen atoms. Combining knowledge of the average amino acid composition with the number of residues in each monomer and number of monomers in the asymmetric unit allows the contribution of the amino acids to the absorption to be calculated. Currently, RADDOSE neglects the crystal rotation when the sample size is larger than the beam size and previously unexposed parts of the crystal rotate into the beam. It also does not yet account for the fluorescence escape: this is only significant for the case of heavy atoms of which there are none in HEWL crystals.

The crystal size was measured with a calibrated light microscope prior to data collection. Since the X-rays from the Osmic optics are convergent, the downstream slit size does not provide an accurate measure of the beam size at the crystal position. This size was measured with X-ray-sensitive green paper glued onto a crystal mounting pin placed on the goniometer head and exposed to X-rays for 30 min. The spot size on the paper was then measured under a light microscope. The results showed that when the slits were set at 1.0 mm by 1.0 mm, the resulting beam size at the crystal position was 0.5 mm in the horizontal direction and 0.3 mm in the vertical direction.

A convergent X-ray beam emerges from the Osmic optics and then passes through two apertures (adjustable in both horizontal and vertical dimensions) attached to the Mar345 goniometer, which are used to reduce scatter and define the physical extent of the beam. Following each aperture, there is an ion chamber giving a reading (in arbitrary units) directly proportional to the number of photons passing through the chamber per second. Prior to data collection, calibration was carried out that allowed ion chamber readings to be converted into an X-ray flux at the crystal position. The calibration was achieved by incrementally increasing the voltage (kV) and current (mA) of the X-ray generator while simultaneously recording both the ion chamber 2 (the chamber closest to the crystal position) and the current induced in a calibrated silicon photodiode (Hamamatsu S3204, 500 μm thick Si) placed at the crystal position. This X-ray-induced current (measured using a picoammeter) can be converted into the number of photons per second by using a known relationship governed by the energy loss of X-rays in silicon, given the beam energy and the thickness of the pin diode (Berger et al., 2005). The calibration (data not shown) was repeated prior to the start of data collection on each crystal,

Table 1. Experimental Parameters for the Eight HEWL Crystals

Crystal	DS	Unit Cell Length (Å) a	c	Δφ (°) per Img	Crystal Size xyz (mm)	Crystal Volume (mm^3)	Res. (Å)	Photon Flux (10^8 ph s^{-1})	Exp. Time per Image (min)	Accum. Irrad. Time (min)	Cumm. Elapsed Time (min)	No. Images per Dataset	Calculated Dose (MGy) Dose	Cum
1	1	79.2	37.9	1.0	0.4 × 0.4 × 0.6	0.096	1.93	1.97	2	180	301	90	0.067	0.067
	3	79.3	37.9	1.0	0.4 × 0.4 × 0.6	0.096	1.93	1.97	2	540	903	90	0.067	0.201
	5	79.7	37.8	1.0	0.4 × 0.4 × 0.6	0.096	1.93	2.02	2	900	1505	90	0.069	0.339
2	1	78.6	38.5	0.6	1.0 × 1.1 × 0.5	0.53	1.93	2.04	3	450	651	150	0.18	0.18
	3	78.4	38.6	0.6	1.0 × 1.1 × 0.5	0.53	1.93	2.05	3	1350	1953	150	0.18	0.54
	5	78.5	38.7	0.6	1.0 × 1.1 × 0.5	0.53	1.93	2.05	3	2250	3255	150	0.19	0.92
	7	78.5	38.8	0.6	1.0 × 1.1 × 0.5	0.53	1.93	2.05	3	3150	4557	150	0.19	1.30
3	1	79.2	37.9	1.0	0.1 × 0.1 × 0.1	0.001	2.07	2.33	13.3	933	1627	70	0.54	0.54
	3	79.6	38.0	1.0	0.1 × 0.1 × 0.1	0.001	2.07	2.33	13.3	2800	4881	70	0.54	1.62
	5	79.3	38.0	1.0	0.1 × 0.1 × 0.1	0.001	2.07	2.33	13.3	4666	8135	70	0.54	2.7
	7	79.0	37.9	1.0	0.1 × 0.1 × 0.1	0.001	2.07	2.33	13.3	6533	11389	70	0.54	3.78
	8	79.4	38.0	1.0	0.1 × 0.1 × 0.1	0.001	2.07	2.33	13.3	7466	13016	70	0.54	4.30
4	1	78.9	38.4	0.4	0.5 × 0.4 × 0.4	0.072	1.93	2.12	3	675	936	225	0.30	0.30
	3	79.0	38.3	0.4	0.5 × 0.4 × 0.4	0.072	1.93	2.15	3	2025	2808	225	0.31	0.91
	5	78.8	38.3	0.4	0.5 × 0.4 × 0.4	0.072	1.93	2.15	3	3375	4680	225	0.30	1.51
	7	78.6	38.5	0.4	0.5 × 0.4 × 0.4	0.072	1.93	2.15	3	4725	6552	225	0.30	2.11
5	1	79.4	37.9	0.9	0.2 × 0.3 × 0.1	0.006	2.03	1.57	10	500	448	50	0.19	0.19
	3	79.4	37.8	0.9	0.2 × 0.3 × 0.1	0.006	2.03	1.61	10	1500	1344	50	0.20	0.59
	5	79.8	38.0	0.9	0.2 × 0.3 × 0.1	0.006	2.03	1.58	10	2500	2688	50	0.20	0.99
	6	79.9	38.0	0.9	0.2 × 0.3 × 0.1	0.006	2.03	1.59	10	3000	3136	50	0.20	1.19
6	1	79.1	38.1	1.0	0.4 × 0.5 × 0.1	0.016	1.93	1.98	2	180	301	90	0.088	0.088
	3	79.1	38.0	1.0	0.4 × 0.5 × 0.1	0.016	1.93	1.98	2	540	903	90	0.088	0.264
	5	79.0	38.0	1.0	0.4 × 0.5 × 0.1	0.016	1.93	1.96	2	900	1505	90	0.087	0.438
	7	79.1	38.0	1.0	0.4 × 0.5 × 0.1	0.016	1.93	1.96	2	1260	2107	90	0.087	0.612
	8	79.2	38.1	1.0	0.4 × 0.5 × 0.1	0.016	1.93	1.96	2	1440	2408	90	0.087	0.699
7	1	79.4	38.0	0.4	0.4 × 0.4 × 0.4	0.064	1.93	2.31	2	450	752	225	0.22	0.22
	3	79.4	38.0	0.4	0.4 × 0.4 × 0.4	0.064	1.93	2.31	2	1350	2256	225	0.22	0.66
	5	79.5	38.0	0.4	0.4 × 0.4 × 0.4	0.064	1.93	2.31	2	2250	3760	225	0.22	1.10
8	1	78.8	38.4	0.6	1.0 × 0.9 × 0.5	0.44	1.93	2.05	3	450	650	150	0.18	0.18
	3	78.8	38.4	0.6	1.0 × 0.9 × 0.5	0.44	1.93	2.05	3	1350	3250	150	0.18	0.54
	5	78.8	38.4	0.6	1.0 × 0.9 × 0.5	0.44	1.93	2.05	3	2250	5850	150	0.18	0.90
	7	78.8	38.6	0.6	1.0 × 0.9 × 0.5	0.44	1.93	2.05	3	3150	8450	150	0.18	1.26

The ϕ sweep was 90° for all crystals except crystal 3 (70°) and crystal 5 (45°). $\Delta\phi$ was 1.0° for crystals 1, 3, and 6, 0.6° for crystals 2 and 8, 0.4° for crystal 4, and 0.9° for crystal 5. The completeness of dataset 1 of all crystals was 100% (100% outer shell). The detector distance was 160 mm for all crystals except crystal 3 (180 mm) and crystal 5 (175 mm). Crystals 1–7 were exposed under a continuous irradiation regime, whereas crystal 8 was exposed under discontinuous irradiation (see text).
The heavy solvent atom concentration of all crystals was 1050 mM l^{-1} of Na and 850 mM l^{-1} of Cl; the number of sulfur atoms per monomer was 10; the number of residues per monomer was 129; the number of monomers per unit cell was 8; the beam size was 0.5 mm horizontally and 0.3 mm vertically; the Gaussian half width was 0.24 mm horizontally and 0.1 mm vertically.

and the photon flux at the crystal position per ion chamber reading remained constant.

Information on the beam profile is also required by RADDOSE: if it is not supplied, a "top hat" beam profile and uniform irradiation across the crystal are assumed. To measure the beam profile at the slit position, the slits furthest from the crystal position were opened as far as possible so that they did not cut down the beam size, and the slits nearest to the beam were slowly moved in the horizontal and vertical directions. This allowed a plot of beam intensity against beam width to be made (which displayed a Gaussian distribution; data not shown) and the FWHM of the beam at the slit position in the horizontal (0.48 mm) and vertical (0.34 mm) directions to be determined. A Gaussian distribution beam profile, which will lead to the differential irradiation of the protein crystal across the profile of the beam, was thus used in RADDOSE. The beam convergence must be accounted for in the determination of beam profile, as the beam profile is measured at the slit position and not at the crystal position. However, as the convergence is known from measuring the beam size both at the slits and at the crystal position (see above) then the Gaussian distribution beam profile at the slits can be scaled down to give the FWHM at the crystal position.

Data Reduction, Processing, and Structure Refinement

All datasets were processed with the CCP4 programming suite (CCP4, 1994). They were integrated between 40 Å and 2 Å resolution with MOSFLM (Leslie, 2006). SCALA (Evans, 2006) was used to scale together multiple observations of reflections, merge multiple observations into an average intensity for a dataset, and assign identical test reflections (for the R_{free} set) for every dataset. TRUNCATE (French and Wilson, 1978) was employed to convert recorded intensities into structure-factor amplitudes. The output files from SCALA were combined together by using CAD, and the datasets from one crystal series were scaled with respect to each other by using Wilson scaling in SCALEIT (Howell and Smith, 1992).

Since the starting PDB model of HEWL (1BWH) (Dong et al., 1999) was derived from a crystal in the same space group and had the same unit cell as for our data, a molecular replacement step was unnecessary. REFMAC5 (Murshudov et al., 1999) was used for rigid body refinement of the model (stripped of all nonprotein atoms) against the first dataset for each crystal, and the program wARP was used to add the water molecules to the models. The water placement and removal was iterated with the maximum-likelihood refinement procedure of REFMAC, as directed by wARP. Restrained refinement was completed by using REFMAC iterated with manual model building by using COOT (Emsley and Cowtan, 2004). The various model analysis tools available in COOT were used to monitor the quality of the refined structure. This information was used to manually alter the model so that the residues sat in the allowed areas of the Ramachandran plot, the density of the $2F_o$-F_c map was well fitted, the number of unusual rotamers were at a minimum, and that there were no significant peaks in the F_o-F_c difference map. This iterative procedure continued until the crystallographic R value < 0.20 and R_{free} < 0.25.

The program CAD was then used to combine the phases from the refined model of dataset 1 for each crystal with the structure factors of the sequential datasets from that crystal, and FFT was used to produce F_{o1}-F_{ox} Fourier difference maps between datasets (where *x* is any dataset other than 1). The Fourier difference maps therefore combined the phases derived from the refined model of dataset 1 and the measured structure factors of each sequential dataset. This process of map production eliminates any dilution of the differences between datasets that would arise during the process of individual refinement of structures against each of the datasets. Peaks showing specific structural damage in the difference maps were used as a criterion for identifying crystals that had undergone radiation damage rather than suffering degradation (and thus loss of diffraction intensity) due to dehydration.

Supplemental Data

Supplemental Data include a full version of Table 1 detailing all collected datasets and typical electron density maps showing the specific damage observed to disulphide bonds observed in structures derived from some room temperature and 100 K data collections, and are available at http://www.structure.org/cgi/content/full/15/12/1531/DC1/.

ACKNOWLEDGMENTS

We would like to thank Ed Lowe for help with data collection, Robin Leslie Owen for cross checking the calibration of our pin diode at the Swiss Light Source, Martin Noble for useful discussions, and the reviewers for their constructive comments. R.J.S.-D. is a Biotechnology and Biological Sciences Research Council-funded Collaborative Awards in Science and Engineering student sponsored by Diamond Light Source, UK. I.C. acknowledges support from Basic Energy Sciences at the United States Department of Energy.

Received: August 11, 2007
Revised: October 4, 2007
Accepted: October 19, 2007
Published: December 11, 2007

REFERENCES

Basavappa, R., Petri, E.T., and Tolbert, B.S. (2003). A quick and gentle method for mounting crystals in capillaries. J. Appl. Crystallogr. *36*, 1297–1298.

Berger, M.J., Hubbell, J.H., Seltzer, S.M., Chang, J., Coursey, J.S., Sukumar, R., and Zucker, D.S. (2005). XCOM: photon cross sections database. (http://physics.nist.gov/xcom).

Blake, C., and Phillips, D.C. (1962). Effects of X-irradiaton on single crystals of myoglobin. In Proceedings of the Symposium on the Biological Effects of Ionising Radiation at the Molecular Level (Vienna: International Atomic Energy Agency), pp. 183–191.

Bonifacic, M., Armstrong, D.A., Carmichael, I., and Asmus, K.-D. (2000). β-fragmentation and other reactions involving aminyl radicals from amino acids. J. Phys. Chem. B *104*, 643–649.

Boutet, S., and Robinson, I.K. (2006). Radiation driven collapse of protein crystals. J. Synchrotron Radiat. *13*, 1–7.

Burmeister, W.P. (2000). Structural changes in a cryo-cooled protein crystal owing to radiation damage. Acta Crystallogr. D Biol. Crystallogr. *56*, 328–341.

CCP4 (Collaborative Computational Project, Number 4) (1994). The CCP4 suite: programs for protein crystallography. Acta Crystallogr. D Biol. Crystallogr. *50*, 760–763.

Cherezov, V., Riedl, K.M., and Caffrey, M. (2002). Too hot to handle? Synchrotron X-ray damage of lipid membranes and mesophases. J. Synchrotron Radiat. *9*, 333–341.

Dong, J., Boggon, T.J., Chayen, N.E., Raftery, J., and Bi, R.C. (1999). Bound-solvent structures for microgravity-, ground control-, gel-, and microbatch-grown hen egg-white lysozyme crystals at 1.8 Å resolution. Acta Crystallogr. D Biol. Crystallogr. *55*, 745–752.

Emsley, P., and Cowtan, K. (2004). Coot: model-building tools for molecular graphics. Acta Crystallogr. D Biol. Crystallogr. *60*, 2126–2132.

Evans, P. (2006). Scaling and assessment of data quality. Acta Crystallogr. D Biol. Crystallogr. *62*, 72–82.

Fletterick, R.J., Sygusch, J., Murray, N., Madsen, N.B., and Johnson, L.N. (1976). Low-resolution structure of the glycogen phosphorylase a monomer and comparison with phosphorylase beta. J. Mol. Biol. *103*, 1–13.

French, G.S., and Wilson, K.S. (1978). On the treatment of negative intensity observations. Acta Crystallogr. *A34*, 517–525.

Garman, E. (1999). Cool data: quantity AND quality. Acta Crystallogr. D Biol. Crystallogr. *55*, 1641–1653.

Garman, E.F., and Schneider, T.R. (1997). Macromolecular cryocrystallography. J. Appl. Crystallogr. *30*, 211–237.

Haas, D., and Rossmann, M.G. (1970). Crystallographic studies on lactate dehydrogenase at −75°C. Acta Crystallogr. B. *26*, 998–1004.

Helliwell, J.R. (1988). Protein crystal perfection and the nature of radiation damage. J. Cryst. Growth *90*, 259–272.

Henderson, R. (1990). Cryo-protection of protein crystals against radiation damage in electron and X-ray diffraction. Proc. R. Soc. Lond. B. Biol. Sci. *241*, 6–8.

Hendrickson, W.A. (1976). Radiation damage in protein crystallography. J. Mol. Biol. *106*, 889–893.

Hendrickson, W.A., Love, W.E., and Karle, J. (1973). Crystal structure analysis of sea lamprey hemoglobin at 2 Å resolution. J. Mol. Biol. *74*, 331–361.

Hill, C.K., Buonaguro, F.M., Myers, C.P., Han, A., and Elkind, M.M. (1982). Fission-spectrum neutrons at reduced dose rates enhance neoplastic transformations. Nature *298*, 67–69.

Hill, C.K., Han, A., and Elkind, M.M. (1984). Fission-spectrum neutrons at a low dose rate enhance neoplastic transformation in the linear low dose region (0-10 cGy). Int. J. Radiat. Biol. Relat. Stud. Phys. Chem. Med. *46*, 11–15.

Hope, H. (1988). Cryocrystallography of biological macromolecules: a generally applicable method. Acta Crystallogr. B *44*, 22–26.

Howell, P.L., and Smith, G.D. (1992). Identification of heavy-atom derivatives by normal probability methods. J. Appl. Crystallogr. *25*, 81–86.

Hug, G.L., Carmichael, I., and Fessenden, R.W. (2000). Direct EPR observation of the aminomethyl radical during the radiolysis of glycine. J. Chem. Soc. Perkin Trans. II *2000*, 907–908.

Kalinin, Y., Kmetko, J., Bartnik, A., Stewert, A., Gillilan, R., Lobkovsky, E., and Thorne, R. (2005). A new sample mounting technique for room-temperature macromolecular crystallography. J. Appl. Crystallogr. *38*, 333–339.

King, M.V. (1958). Improved resolution of X-ray diffraction patterns of protein crystals at low temperature. Nature *181*, 263–264.

Kmetko, J., Husseini, N., Naides, M., Kalinin, Y., and Thorne, R. (2006). Quantifying X-ray radiation damage in protein crystals at cryogenic temperatures. Acta Crystallogr. D Biol. Crystallogr. *62*, 1030–1038.

Koufen, P., Brdiczka, D., and Stark, G. (2000). Inverse dose-rate effects at the level of protiens observed in the presence of lipids. Int. J. Radiat. Biol. *76*, 625–631.

Krokosz, A., Koziczak, R., Gonciarz, M., and Szweda-Lewandowska, Z. (2006). Study of the effect of dose-rate on radiation-induced damage to human erythrocytes. Radiat. Phys. Chem. *75*, 98–105.

LaVerne, J.A. (2000). OH radicals and oxidizing products in the gamma radiolysis of water. Radiat. Res. *153*, 196–200.

Leiros, H.K.S., McSweeney, S.M., and Smalas, A.O. (2001). Atomic resolution structures of trypsin provide insight into structural radiation damage. Acta Crystallogr. D Biol. Crystallogr. *57*, 488–497.

Leiros, H.K.S., Timmins, J., Ravelli, R., and McSweeny, S. (2006). Is radiation damage dependent on the dose rate used during macromolecular data collection? Acta Crystallogr. D Biol. Crystallogr. *62*, 125–132.

Leslie, A.G.W. (2006). The integration of macromolecular diffraction data. Acta Crystallogr. D Biol. Crystallogr. *62*, 48–57.

Mozumder, A., and Magee, J.L. (1966). Theory of radiation chemistry. VII. Structure and reaction in low LET tracks. J. Chem. Phys. *45*, 3332–3341.

Murray, J., and Garman, E. (2002). Investigation of possible free-radical scavengers and metrics for radiation damage in protein crystallography. J. Synchrotron Radiat. *9*, 347–354.

Murray, J.W., Garman, E.F., and Ravelli, R.B.G. (2004). X-ray absorption by macromolecular crystals: the effects of wavelength and crystal composition on absorbed dose. J. Appl. Crystallogr. *37*, 513–522.

Murray, J.W., Rudino-Pinera, E., Owen, R.L., Grininger, M., Ravelli, R.B., and Garman, E.F. (2005). Parameters affecting the X-ray dose absorbed by macromolecular crystals. J. Synchrotron Radiat. *12*, 268–275.

Murshudov, G.N., Lebedev, A., Vagin, A.A., Wilson, K.S., and Dodson, E.J. (1999). Efficient anisotropic refinement of macromolecular structures using FFT. Acta Crystallogr. D Biol. Crystallogr. *55*, 247–255.

Nave, C., and Garman, E. (2005). Towards an understanding of radiation damage in cryocooled macromolecular crystals. J. Synchrotron Radiat. *12*, 257–260.

O'Neill, P., Stevens, D.L., and Garman, E. (2002). Physical and chemical considerations of damage induced in protein crystals by synchrotron radiation: a radiation chemical perspective. J. Synchrotron Radiat. *9*, 329–332.

Owen, R.L., Rudino-Pinera, E., and Garman, E.F. (2006). Experimental determination of the radiation dose limit for cryocooled proteins. Proc. Natl. Acad. Sci. USA *103*, 4912–4917.

Phillips, J.C., Wlodawer, A., Yevitz, M.M., and Hodgson, K.O. (1976). Applications of synchrotron radiation to protein crystallography: preliminary results. Proc. Natl. Acad. Sci. USA *73*, 128–132.

Pimblott, S.M., LaVerne, J.A., Bartels, D.M., and Jonah, C.D. (1996). Reconciliation of transient absorption and chemically scavenged yields of the hydrated electron in radiolysis. J. Phys. Chem. *100*, 9412–9415.

Ravelli, R.B., and Garman, E. (2006). Radiation damage in macromolecular crystallography. Curr. Opin. Struct. Biol. *16*, 624–629.

Ravelli, R.B.G., and McSweeney, S.M. (2000). The 'fingerprint' that X-rays can leave on structures. Structure *8*, 315–328.

Ravelli, R.B.G., Theveneau, P., McSweeney, S., and Caffrey, M. (2002). Unit-cell volume change as a metric of radiation damage in crystals of macromolecules. J. Synchrotron Radiat. *9*, 355–360.

Rodgers, D.W. (1997). Practical cryocrystallography. Methods Enzymol. *276*, 183–203.

Singh, A., and Singh, H. (1982). Time-scale and nature of radiation-biological damage: approaches to radiation protection and post-irradiation therapy. Prog. Biophys. Mol. Biol. *39*, 69–107.

Skrzypczak-Jankun, E., Bianchet, M.A., Amzel, L.M., and Funk-Jnr, M.O. (1996). Flash-freezing causes a stress-induced modulation in a crystal structure of soybean lipoxygenase L3. Acta Crystallogr. D Biol. Crystallogr. *52*, 959–965.

Sliz, P., Harrison, S.C., and Rosenbaum, G. (2003). How does radiation damage in protein crystals depend on X-Ray dose? Structure *11*, 13–19.

Snell, E.H., Bellamy, H.D., Rosenbaum, G., and van der Woerd, M.J. (2007). Non-invasive measurement of X-ray beam heating on a surrogate crystal sample. J. Synchrotron Radiat. *14*, 109–115.

Stark, G. (1991). The effect of ionizing radiation on lipid membranes. Biochim. Biophys. Acta *1071*, 103–122.

Sygusch, J., and Allaire, M. (1988). Sequential radiation damage in protein crystallography. Acta Crystallogr. A *44*, 443–448.

Sykes, C.E., and Watt, D.E. (1989). Interpretation of the increase in frequency of neoplastic transformations observed for some ionising radiations at low dose rates. Int. J. Radiat. Biol. *55*, 925–942.

Teng, T. (1990). Mounting of crystals for macromolecular crystallography in a free-standing thin film. J. Appl. Crystallogr. *23*, 387–391.

Weik, M., Ravelli, R.B.G., Kryger, G., McSweeney, S., Raves, M.L., Harel, M., Gros, P., Silman, I., Kroon, J., and Sussman, J.L. (2000). Specific chemical and structural damage to proteins produced by synchrotron radiation. Proc. Natl. Acad. Sci. USA *97*, 623–628.

Wilson, K.S., Stura, E.A., Wild, D.L., Todd, R.J., Stuart, D.I., Babu, Y.S., Jenkins, J.A., Standing, T.S., Johnson, L.N., Fourme, R., et al. (1983). Macromolecular crystallography with synchrotron radiation. II. Results. J. Appl. Crystallogr. *16*, 28–41.

Wisniowski, P., Carmichael, I., Fessenden, R.W., and Hug, G.L. (2002). Evidence for β-scission in the oxidation of amino acids. J. Phys. Chem. A *106*, 4573–4580.